scientific reports

Check for updates

OPEN

Selective nanocomposite hydrogels developed from cashew gum/laponite for selective removal

Albert Santos Silva[1], Ariane Maria Silva Santos[1], Josy Anteveli Osajima[1], Edvani Curti Muniz[1], Monica Felts de La Roca Soares[2], Rafael Felippe Ratke[3], Natielly Pereira da Silva[3] & Edson C. Silva-Filho[1]✉

Dyes are significant pollutants in aquatic environments, even at low concentrations. To address this issue, superabsorbent nanocomposite hydrogels were developed using cashew tree gum cross-linked with acrylamide and incorporating laponite as a selective adsorbent for cationic dyes. The hydrogels were characterized through Fourier Transform Infrared Spectroscopy (FTIR), Thermogravimetric Analysis (TG), X-ray Diffraction (XRD), Scanning Electron Microscopy (SEM), and Energy-Dispersive Spectroscopy (EDS), along with assessments of toxicity, swelling capacity, and adsorption parameters. TG and XRD analysis indicated the incorporation of laponite into the polymer matrix. FTIR showed no significant changes due to the low concentration of laponite. SEM revealed a uniform surface in the laponite-containing hydrogel (HGC-LAP). EDS confirmed the presence and good distribution of Mg and Si elements in HGC-LAP. Although hydrogels without laponite (HGC) showed higher swelling capacity, HGC-LAP demonstrated faster adsorption kinetics, with values approaching those of HGC at equilibrium. The addition of laponite improved the adsorption capacity to 2887.5 mg g^{-1}, and the data fitted the pseudo-second order and Langmuir models. The nanocomposite hydrogels proved to be effective as selective adsorbents in dye mixtures.

Keywords Polysaccharide, Adsorption, Water treatment, Selectivity

Rapid industrial development has caused serious problems for the environment due to waste disposal without a post-treatment stage. This has caused pollution of aquatic environments through the dumping of waste from industry, introducing substances into the aquatic environment that are difficult to degrade and affecting the entire ecosystem[1–3]. The effluents of many industries such as paint industries, food industries, pharmaceutical industries, and battery manufacturing, that contain heavy metal ions, dyes, and organic materials, are discharged directly into water resources[4,5]. One of the components responsible for major pollution in aquatic environments are dyes, which are highly important substances in industry, frequently used in the textile, paper, food, rubber and cosmetics areas, with a wide variety of compounds, exceeding the value of 100,000 compounds[6]. Due to their high industrial demand, dyes are a cause for environmental concern, as it is estimated that 15% of the volume produced is discarded in inappropriate places, causing irreversible environmental damage or difficult to resolve, directly affecting water sources and the entire environment used this natural resource[6]. Problems caused by dumping into bodies of water include: (i) change in color, reduction in photosynthesis due to reduced incidence of light; and (ii) increased toxicity even at low concentrations[7]. Researchers have always been looking for the best and most economical methods to remove pollutants[8,9], some methods are used to remove pollutants in aquatic environments, such as adsorption, coagulation and flocculation, reverse osmosis, chemical oxidation, and physical methods such as membrane filtration. They are inefficient for the complete removal of dyes and are expensive[10]. Among these methods, adsorption becomes an economically viable alternative, easy to apply, in addition to high efficiency when compared to other methods[1,3].

Superabsorbent hydrogels stand out in adsorption due to their excellent characteristics, being able to be synthesized from natural polymers and having a high capacity for removing pollutants[1,11]. Superabsorbent hydrogels are materials with high water absorption capacity due to the chemical nature of their bonds, due to the presence of hydrophilic groups[1,2]. Superabsorbent hydrogels have the ability to retain fluids between their

[1]Interdisciplinary Laboratory for Advanced Materials, LIMAV, Piaui Federal University, Ministro Petronio Portella University Campus, Teresina, Piaui 64049-550, Brazil. [2]Department of Pharmaceutical Sciences, Drug Quality Control Center, Recife 50670-901, Brazil. [3]University of Mato Grosso do Sul, Chapadão do Sul, MS 79560-000, Brazil. ✉email: edsonfilho@ufpi.edu.br

chains without dissolving the polymeric structure. This absorption capacity can be controlled through porosity, crosslinking density and by alkaline hydrolysis[1,12]. Furthermore, its highly expandable structure allows the adsorption of contaminants through interaction with functional groups[13].

Hydrogels can be classified according to several specific characteristics, including origin, morphology, type of crosslinking and appearance[14]. In general, chemical hydrogels are formed by the crosslinking of one or more types of monomers, which may be of synthetic or natural origin (or a mixture of these in varying proportions), in addition to the presence of a reaction initiation radical, catalyst and crosslinking agent[14]. Natural polymers have been widely used to prepare new materials because they have high biodegradability, biocompatibility and are non-toxic. Furthermore, they are obtained from renewable sources, unlike synthetic polymers that are produced through petrochemical sources that can take centuries to decompose in the environment[15]. The gum extracted from the cashew tree is a biopolymer found in the trunk and branches of the tree itself and is soluble in water. This gum is considered a complex polysaccharide composed of rhamnose, arabinose, xylose, galactose, glucose, glucuronic acid and sugar residues[16]. As it is extracted from a plant easily found in the northeast region of Brazil, the use of cashew tree gum, as a natural polymer, is directly linked to its extraction efficiency and uses and, at the same time, is an economically attractive proposal for the Brazilian scenario[12,16–18].

Hydrogels are a new class of adsorbents widely applied to decontaminate wastewater[19,20]. The adsorption capacity of cationic dyes can be enhanced through the use of nanocomposite hydrogels containing inorganic materials, such as laponite, a synthetic clay mineral with a chemical formula $Na_{0,7}Si_8Mg_{5,5}Li_{0,3}O_{20}(OH)_4$ in which tetrahedral sheets of SiO^2 are coordinated with a sheet of Mg ions[21,22]. Clay is a abundant material that is easily extracted and has good mechanical and chemical properties and is used in wastewater treatment[23,24]. Laponite is made up of particles that have a negatively charged surface and have the ability to form a gel in water, although with a weak interaction, but which can be used in the synthesis of new superabsorbent hydrogels, thus increasing the adsorption capacity for dyes[22]. This clay mineral has a negatively charged surface, and has a high surface area, which makes it a material capable of adsorbing molecules on its surface. When associated with polymers, to form a nanocomposite, an increase in properties or synergism can occur, also providing selectivity in adsorption processes, a characteristic that makes the new nanocomposite an applicable product, since in nature pollution occurs in environments where there is a mixture of several pollutants[25], and selectivity is often of extreme importance and most materials do not present this property. The association of laponite with the cross-linked chain of a hydrogel can bring several benefits such as greater swelling kinetics, that is, greater speed of water absorption with irrelevant losses in absorption capacity. The insertion of laponite into hydrogels also provides improvements in other properties, such as mechanical and thermal resistance, which can be controlled with controllable dosages of the clay mineral to achieve the properties for each desired application. For adsorption processes, the formation of the nanocomposite with laponite from 1% already guarantees synergism and increased selectivity in dyes or other molecules[25].

Therefore, this work aims to synthesize hydrogels from the chemical crosslinking of cashew tree gum with acrylamide containing Laponite for the adsorption of cationic dyes. The hydrogels produced were characterized by FTIR, XRD, TG, SEM, EDS, in addition to swelling and toxicity tests. Several adsorption parameters were evaluated, such as the influence of pH, zero charge point, contact time and concentration, in addition to the application of kinetic and equilibrium models.

Materials and methods

Materials

The materials used for the development of this work include acrylamide, 98% (Aldrich), potassium persulfate ($K_2S_2O_8$), 99.0% (Aldrich), N, N'-methylene-bisacrylamide (MBA), 99.0% (Aldrich), N, N, N ', N'–tetramethylenediamine (TEMED), 99.9% (Aldrich), sodium hydroxide 99% (Dynamics), potassium bicarbonate ($KHCO_3$) (Dynamics), ethyl alcohol (C_2H_5OH), 99.8% (Dynamics), methyl alcohol (CH3OH) 99.8% (Dynamics), crystal violet dye ($C_{24}H_{28}N_3Cl$) and methyl orange ($C_{14}H_{14}N_3NaO_3S$) (Dynamics), hydrochloric acid (Dynamics), sodium chloride (NaCl) (Dynamic), Magnesium Chloride (MgCl), Magnesium Sulfate ($MgSO_4$), Calcium Chloride ($CaCl_2$) (Dynamic), Potassium Chloride (KCl) (Dynamic), Sodium Bicarbonate ($NaHCO_3$) (Dynamic) gum exudate of cashew extracted (Teresina – Piauí; - SISGEN: ABD61DA) and deionized water.

Purification of cashew tree exudate and nanocomposite synthesis

The isolation and purification of cashew tree exudate (*Anacardium occidentale L*) was carried out following the methodology of Rodrigues et al., (1993), with some adaptations, as shown in Fig. 1[26]. The cashew tree gum hydrogel synthesis process was carried out according to the methodology of Rodrigues et al., (2021)[12]. The hydrogels containing the clay mineral Laponite were synthesized following the HGC methodology, with the addition of 0.1 g of Laponite in the step prior to the addition of acrylamide, left stirring for 5 min. The schematization of the synthesis of nanocomposites then described in Fig. 1.

Swelling test

For the swelling test, 0.020 g of each of the hydrogels was immersed in 10.0 mL of distilled water at a temperature of 25 °C for predefined periods between 30 and 120 min, after each time, the excess water was removed with the aid of filter paper and then the swelling ratio for each sample was determined according to Eq. 1[27]:

$$Swelling = \frac{C_f - C_i}{C_i}\ x\ 100 \tag{1}$$

Where C_i and C_f are the mass of the hydrogel before and after swelling, respectively.

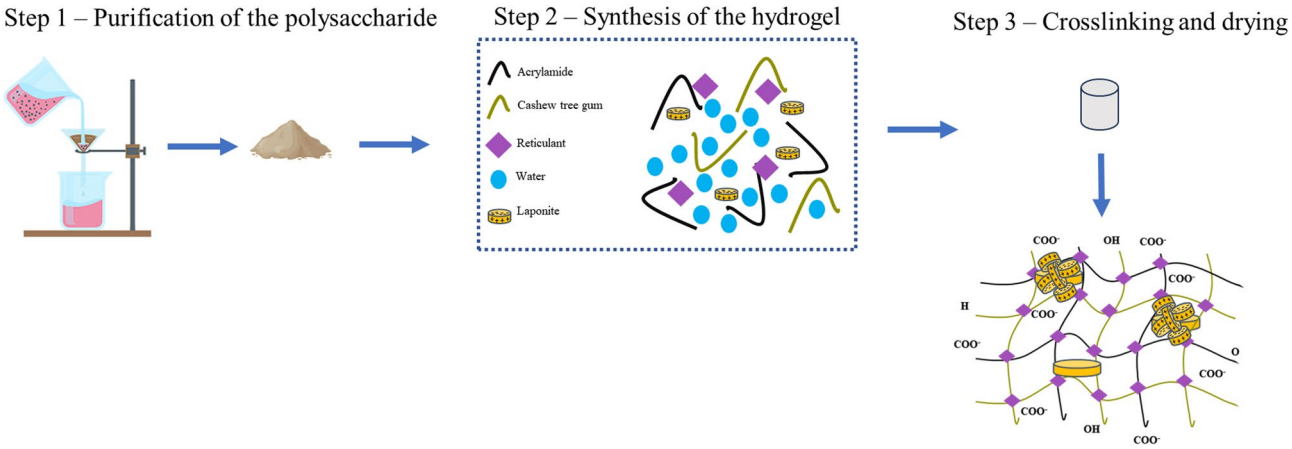

Fig. 1. Illustration of the cashew tree gum purification process and nanocomposite synthesis.

Toxicity

The toxicity test against *Artemia salina* was carried out following the methodology proposed by Meyer et al., (1982) with some modifications[28].

The solutions were prepared in triplicate ($n = 3.0$) and tested at concentrations of 0.1 to 5.0 mg mL^{-1}, with 10.0 nauplii of *A. salina* being added per flask, and survivors were counted after 48.0 h.

To test the material after adsorption, 10.0 nauplii of *A. Saline* were added to a solution containing 2.5 mL of the saline solution and 2.5 mL of the supernatant after the adsorption process. The count was carried out after 48 h.

Characterizations

To determine the crystallographic profile, X-ray Diffraction (XRD) equipment from SHIMADZU, model XRD-6000 with CuKα radiation (λ = 1.54 Å) was used. The analyzes were performed operating in the 2θ range of 5° to 75°, with a scan rate of 2° min^{-1}.

The infrared spectra were obtained using Vertex 70v equipment from Bruker, with 120 scans and a range of 4000 to 400 cm^{-1} and a resolution of 4 cm^{-1}. Measurements were made for transmission using potassium bromide (KBr).

Thermogravimetric analyzes and their derivatives were carried out in the temperature range between 10 and 800 °C and heating rates of 10 °C min^{-1}, under an argon atmosphere, on the TA Instruments SDT-600 equipment.

Microscopies were performed using a field emission scanning electron microscope (FESEM) (QUANTA 250 FEI, FEI Company, Eindhoven, Netherlands) together with elemental analysis by energy dispersive spectroscopy (EDS) (EDAX Apollo X, FEI Company, Eindhoven, Netherlands).

Effects of pH

The effect of pH on the adsorption of crystal violet dye was studied at pHs 2, 4, 6, 8 and 10, in triplicates ($n = 3$), at a temperature of 25 °C. The pH of the solutions were adjusted with the addition of NaOH and/or HCl at 0.1 and 0.5 mol L^{-1}. pH measurements were performed on a pHS-3E pH meter. Calibration was carried out using buffer solutions of pH 4.0 and 7.0. The experiments were conducted in a 50.0 mL Erlenmeyer flask containing 10.0 mg of hydrogels with and without laponite and a volume of dyes of 30.0 mL and a concentration of 1000 ppm. The Erlenmeyer flasks were placed in an incubator with orbital shaking for 2 h at 110 rpm and a temperature of 25 °C. Subsequently, the solutions were centrifuged and the supernatant concentrations were determined by ultraviolet visible (UV-Vis) spectroscopy. The adsorption capacity was determined using Eq. 2.

$$q = \frac{(C_i - C_e) \times V}{m} \tag{2}$$

Where q is the adsorption capacity (mg g^{-1}), Ci and Ce are the concentrations of the dyes before and after adsorption (mg L^{-1}), V is the volume of the solution (L) and m represents the amount of hydrogel used (g).

Adsorption kinetics

The adsorption kinetic tests were carried out in triplicate ($n = 3$), at a temperature of 25 °C and natural pH of the dye solution (6.0). Initially, 10 mg of hydrogels were added to 30.0 mL of dye solutions and kept under constant stirring at 110 rpm for periods of 5 to 240 min[7]. After the contact time, the samples were centrifuged and the supernatant concentration determined in a UV-Vis spectrophotometer and the adsorption capacity was determined according to Eq. 2. The pseudo-first order and pseudo-second order models were used for analysis of experimental data. The pseudo-first order kinetic Eq. 3[1] is given as:

$$q_t = q_e(1 - e^{-kt}) \tag{3}$$

Where k_1 is the model adsorption rate constant (min^{-1}), qe and qt are the adsorption capacities at equilibrium and at time *t* (min). The pseudo-second order Eq. 3[2] is given by:

$$q_t = \frac{kq_e^2 t}{1 + kq_e t} \tag{4}$$

Where k_2 is the constant of the pseudo-second order kinetic model (g mg^{-1} min^{-1}).

Adsorption isotherms

The test was carried out in triplicate at 25 °C, with pH adjusted according to the best adsorption. 10.0 mg of lyophilized hydrogels were added to 30.0 mL of dyes, varying concentrations between 50 and 1000 mg L^{-1}, which were stirred at the best equilibrium time found in the kinetic experiment[7].

The Langmuir and Freundlich adsorption isotherms were used to evaluate the experimental data on the adsorption equilibrium. Equation 5 describes the Langmuir equation, where q_e is the amount of dye adsorbed per mass of adsorbent (mg g^{-1}) and q_m the amount adsorbed (mg g^{-1}), represents the adsorbate concentration at equilibrium (mg L^{-1}), and $_L$ is the Langmuir adsorption constant related to the equilibrium between adsorbate and adsorbent (L mg^1)[31].

$$q_e = \frac{q_m K_L C_e}{1 + K_L C_e} \tag{5}$$

Equation 6 describes the Freundlich equation, where K_f is the Freundlich adsorption constant related to the adsorption capacity and is the parameter related to the intensity of the adsorption process, which represents the amount of dye adsorbed (mg g^{-1}), e is the equilibrium concentration of the adsorbate (mg L^{-1})[32].

$$q_e = K_f C_e^{1/n} \tag{6}$$

Equation 7 describes the Redlich-Peterson isotherm[33], which is a combination of the Langmuir-Freundlich model, where the exponent β varies between 0 and 1 and is characterized by the best fit to the Langmuir model when β = 1 and to the Freundlich model when β = 0. In the Redlich-Peterson model, K_R (L g^{-1}), $\propto_R$ (L mg^{-1}), and β are constants of the Redlich-Peterson isotherm.

$$q_e = \frac{K_R C_e}{1 + \propto_R C_e^{\beta}} \tag{7}$$

The Sips isotherm, Eq. 8[34], is a model that combines the Langmuir and Freundlich isotherms and is used to describe heterogeneous surfaces where the adsorption energy is not constant, unlike what is described by Langmuir, but varies as described by the Freundlich isotherm. In the Sips isotherm, K_S is the constant related to adsorption capacity (mg g^{-1}) and n defines the affinity related to the Langmuir and Freundlich isotherms, where when $n = 1$, the Sips isotherm reduces to Langmuir, and when $n < 1$, it indicates greater heterogeneity on the adsorbent surface as described by the Freundlich equation. When $n > 1$, it indicates cooperative behavior, where adsorption is favored as more molecules are adsorbed.

$$q_e = \frac{Q_{max} K_S C_e^{1/n}}{1 + K_S C_e^{1/n}} \tag{8}$$

The Temkin isotherm, described in Eq. 9[35], describes the adsorption mechanism when the surface has a distribution of energy, considering a linear decrease in adsorption as the amount of solute increases. In the Temkin equation, A is the constant related to adsorption capacity (L g^{-1}), and B is the constant related to interactions between the adsorbed molecules (J/mol).

$$q_e = Bln(AC_e) \tag{9}$$

The Dubinin-Radushkevich isotherm, Eq. 10[36],is used to describe adsorption in porous materials where physical adsorption is predominant. Here, R is the universal gas constant (8.314 J $(mol.K)^{-1}$) and T is the temperature in Kelvin (K).

$$q_e = q_m e^{RTln(1+\frac{1}{C_e})} \tag{10}$$

Results and discussion

Laponite differs from other clay minerals because it is synthetic and has lower crystallinity[37]. Due to this, as observed in Fig. 2a, laponite shows broad diffraction peaks at 5.62°, 19.74°, 28.10°, 35.16°, 53.47°, 61.03° and 72.17°.

According to Ferreira et al., (2019) cashew tree gum has microcrystalline regions in the regions of 2θ = 15.11°, 17.54° and 23.06°[38]. Furthermore, it may vary depending on the region where the material is obtained. Analyzing the HGC data, a relationship is observed in the profile between cashew tree gum, observed by Ferreira et al.,

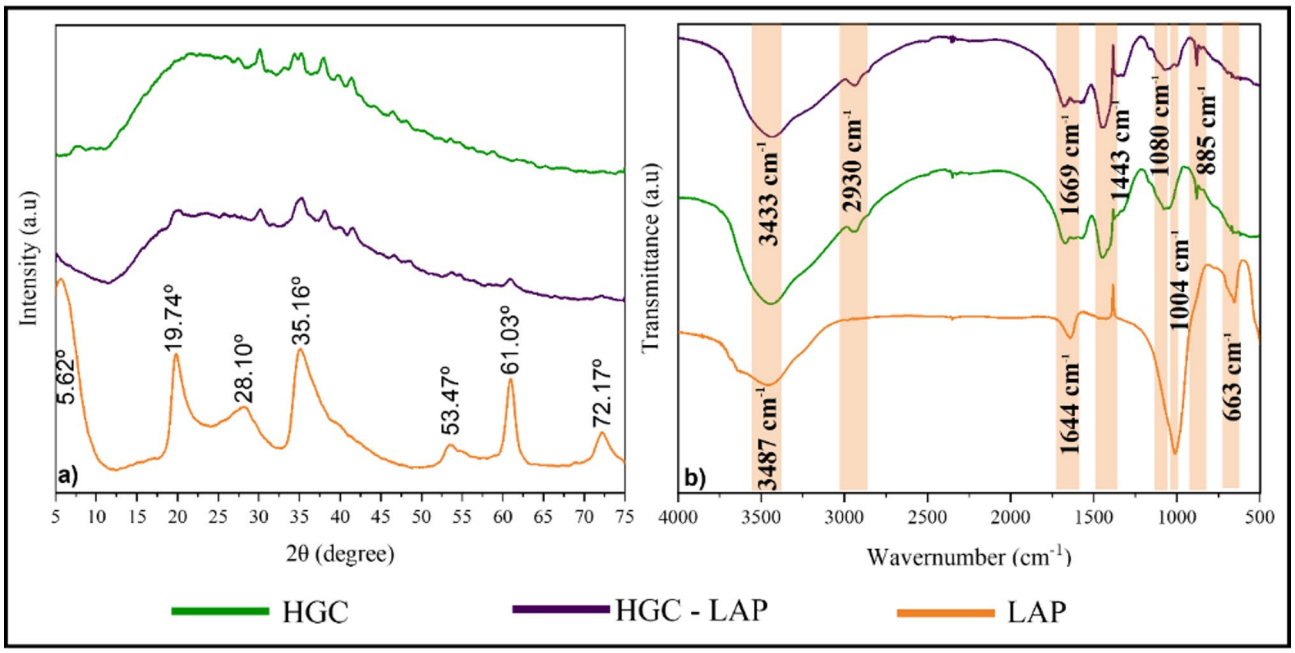

Fig. 2. (a) X-ray diffraction pattern and (b) FTIR spectra for HGC, HGC-LAP and LAP.

(2019) and polyacrylamide already considered by Rodrigues et al., (2021), which may be related to the effect of the occurrence of copolymerization between polyacrylamide and cashew tree gum[12].

The HGC-LAP presented diffraction patterns similar to the HGC, but with the appearance of diffraction peaks at 5.62º, 19.74º, 28.10º, 35.16º, 53.47º, 61.03º and 72.17º, due to the presence of laponite, indicating that the polymeric cross-linking reaction promoted chains interconnected with laponite[16].

The FTIR spectra for identifying the functional groups present in the materials were investigated and are described in Fig. 2b. The HGC and HGC-LAP spectra showed characteristic bands referring to cashew tree gum and polyacrylamide[12]. The bands observed between 3600 and 3000 cm^{-1} are attributed to the superposition of the N-H and O-H stretching vibration resulting from the presence of physically bound water, causing an expansion of the band in this range.

The band located at 2930 cm^{-1} is due to the asymmetric and symmetric stretching of the C-H present in the biopolymer. The band present at 1669 cm^{-1} corresponds to the stretching of C = O and vibration of N-H present in polyacrylamide, having a low intensity due to the occurrence of hydrolysis, where the conversion of amide groups (-$CONH_2$) into carboxylate groups occurs (-COO)[12]. Other bands located at 1443 cm^{-1} refer to the stretching of N-H, at 1080 cm^{-1} related to C-O-C glycosidic bonds and O-H bending of alcohols and at 885 cm^{-1} corresponding to the C-H bending vibration, present in the gum structure of the cashew tree[12].

For the Laponite spectrum, absorption bands were identified located at 1004 and 663 cm^{-1}, referring to the stretching vibration mode of the Si-O-Si and Mg(Li)-O(OH) groups respectively[22]. The absorption bands located between 3600–3100 cm^{-1} and 1630 cm^{-1} are related to the OH groups bonded by hydrogen and water of hydration. The spectra of HGC-LAP differ from HGC due to the appearance of the absorption band in the region of 1004 cm^{-1}, characteristic of the vibration of Si-O-Si groups, proving the presence of clay mineral in the structure of the material[22], as already verified in XRD.

The morphology of the hydrogels was analyzed using SEM, along with the identification of specific elements through EDS in the regions corresponding to the micrographs, with the results presented in Fig. 3. The HGC micrograph (Fig. 3) shows a surface with roughness and interconnected spaces. This characteristic contributes to an increased final swelling rate of the material[12]. However, despite this feature, the swelling capacity of both materials was similar, likely due to interactions with water also involving the clay mineral. The HGC-LAP micrograph (Fig. 3) shows a more uniform surface than that of HGC, without surface cracks. This feature is associated with the densification of the structure due to the presence of laponite. The EDS mapping analysis for HGC-LAP indicates the presence of laponite in the polymer matrix, evidenced by homogeneous regions of Si, O, and Mg. Furthermore, the mapping showed a uniform distribution of these elements, suggesting good dispersion of laponite within the matrix, which may contribute to improved mechanical and structural properties of the hydrogel[21].

The thermal characterization of HGC and HGC-LAP is shown in Fig. 4. From the thermogravimetric curves it is possible to observe the thermal events occurring in the materials. The TG curve of Laponita, Fig. 4a, showed a thermal event at 67 ºC and 6.8% mass loss due to the release of water and volatile compounds adsorbed on the surface[39].

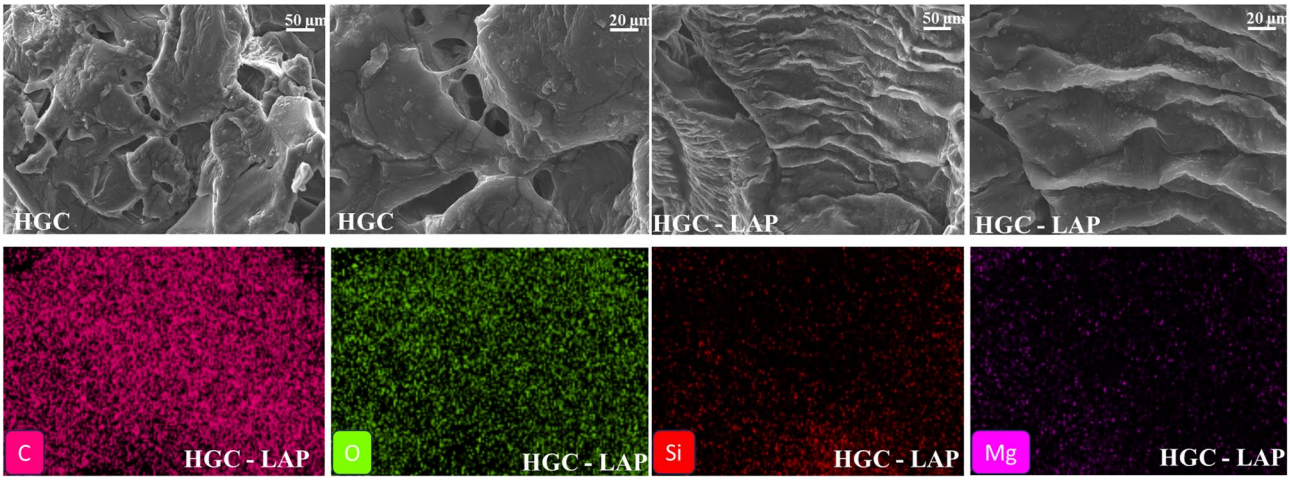

Fig. 3. Microscopy for samples at different magnifications and EDS for HGC and HGC-LAP samples.

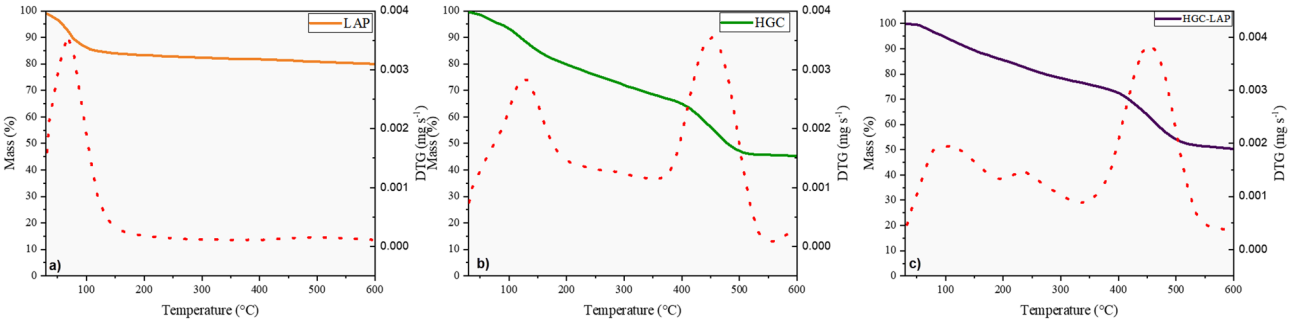

Fig. 4. Thermogravimetric curves and derivatives: (a) LAP. (b) HGC and (c) HGC-LAP.

The HGC system, Fig, 4b and HGC-LAP Fig. 4c showed three thermal events. The first event of the HGC occurred at 123 °C with a mass loss of 10.25% while the HGC-LAP the first occurs at 99.43 °C with a loss of 4.99% while the second occurs at a temperature of 237.49 °C and mass loss 15.51%, both related to loss of water and volatile gases. These data suggest proof of the presence of laponite in the HGC-LAP structure, since a lower mass loss is observed in this system because the inorganic fillers dispersed in the polymeric matrix act as a barrier in the mass transport for the products generated in the decomposition of the polymer phase[39].

The greatest mass loss was observed at temperatures of 450 and 456 °C for HGC and HGC-LAP respectively, due to decomposition reactions of the polymeric chain of the hydrogels[40]. It is observed that HCG-LAP presents a lower mass loss compared to HGC, thus proving the presence of inorganic matter in the matrix of this hydrogel, which was added at a rate of 2% and is still present at this temperature.

Swelling

Hydrogels are materials that have a high water absorption capacity due to the presence of hydrophilic chains that make up the polymer. Parameters such as polymer chain density can interfere with the way these materials absorb aqueous solutions[1,13].

Figure 5 shows the capacity of hydrogels to absorb water, up to a period of 120 min, where swelling equilibrium occurred. HGC showed a progressive increase in absorption, presenting a maximum absorption of approximately 22,000%, while HGC-LAP had an absorption close to maximum of approximately 20,000% within 30 min.

The addition of an inorganic filler to the hydrogel matrix causes an increase in the crosslinking density, resulting in a decrease in the water absorption of HGC-LAP in relation to HGC[12,41,42], however laponite differs from the vast majority of fillers inorganic, as it has the capacity to form gels, and maintains its negatively charged form due to the presence of silanol groups (Si-O-) not influencing swelling in a way that greatly reduces this capacity, when compared to other clay minerals, for example[21,25].

Effect of contact time

The influence of contact time was evaluated on the hydrogels in a range of 5 to 240 min with a dye concentration of 150 mg^{-1} and pH 6, as shown in Fig. 6. HGC showed lower adsorption when compared to HGC-LAP.

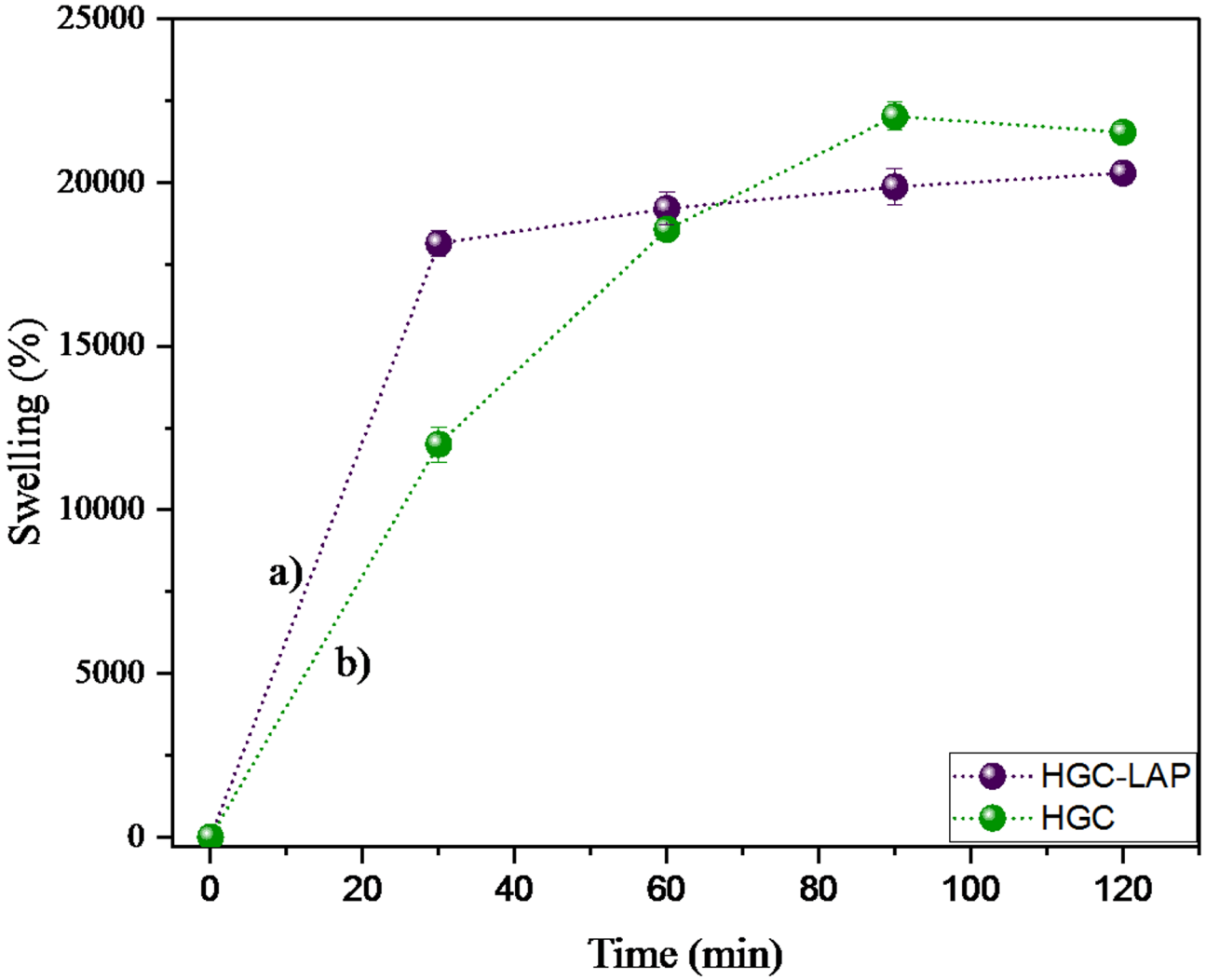

Fig. 5. Sample swelling capacity: (a) HCG-LAP (b) HCG.

In Fig. 6 it is possible to observe a rapid slope in the curve up to a time of 30 min, due to the high availability of active sites present in both materials, with a high adsorption rate more evident for HGC-LAP due to the clay mineral, entering in balance in the first 30 min. As the sites are filled, the adsorption rate decreases due to electrostatic repulsion between the dye molecules. HGC presented a different profile, entering adsorption equilibrium only after 240 min.

The data obtained in the adsorption kinetics are similar to that of water absorption, where equilibrium occurs first for the material containing laponite, due to the greater number of active sites for adsorption of the cutting agent and water, provided by the presence of the clay mineral[25].

The experimental data in Fig. 6 were modeled based on pseudo-first-order and pseudo-second-order equations in order to observe the mechanisms involved in the interaction between the adsorbent matrix and the crystal violet dye[29,30]. The dye concentration used in the test was 150 ppm, referring to one of the points obtained for the concentration isotherms. The adjustment was applied based on the adsorption equilibrium, with 30 min for HGC-LAP and 240 min for HGC are described in Table 1.

As seen in Table 1, there is a greater fit to the pseudo-second order kinetics model in both HGC and HGC-LAP materials, indicating that chemisorption is the rate limiting step[7].

From the data in Table 1, a higher R^2 value was observed for the pseudo-second order model for both hydrogels, in addition to the equilibrium adsorption capacity found through the model being close to the experimental value. The pseudo-first order model did not fit well for the HGC, as the R^2 was lower than the other model. For HGC-LAP, the R^2 was 0.97, however there was a large difference between the experimental and calculated adsorbed amount.

Hydrogels for removing cationic dyes have been described in the literature mentioning R^2 values close to 1 for this model[7,43]. From this, it is suggested that the interaction process between the adsorbate and adsorbent is a chemical process where the sharing or exchange of electrons is the rate-limiting step[44]. From these kinetic data, the synergisms between laponite and the hydrogel stand out, as already reported in other nanocomposite materials[25].

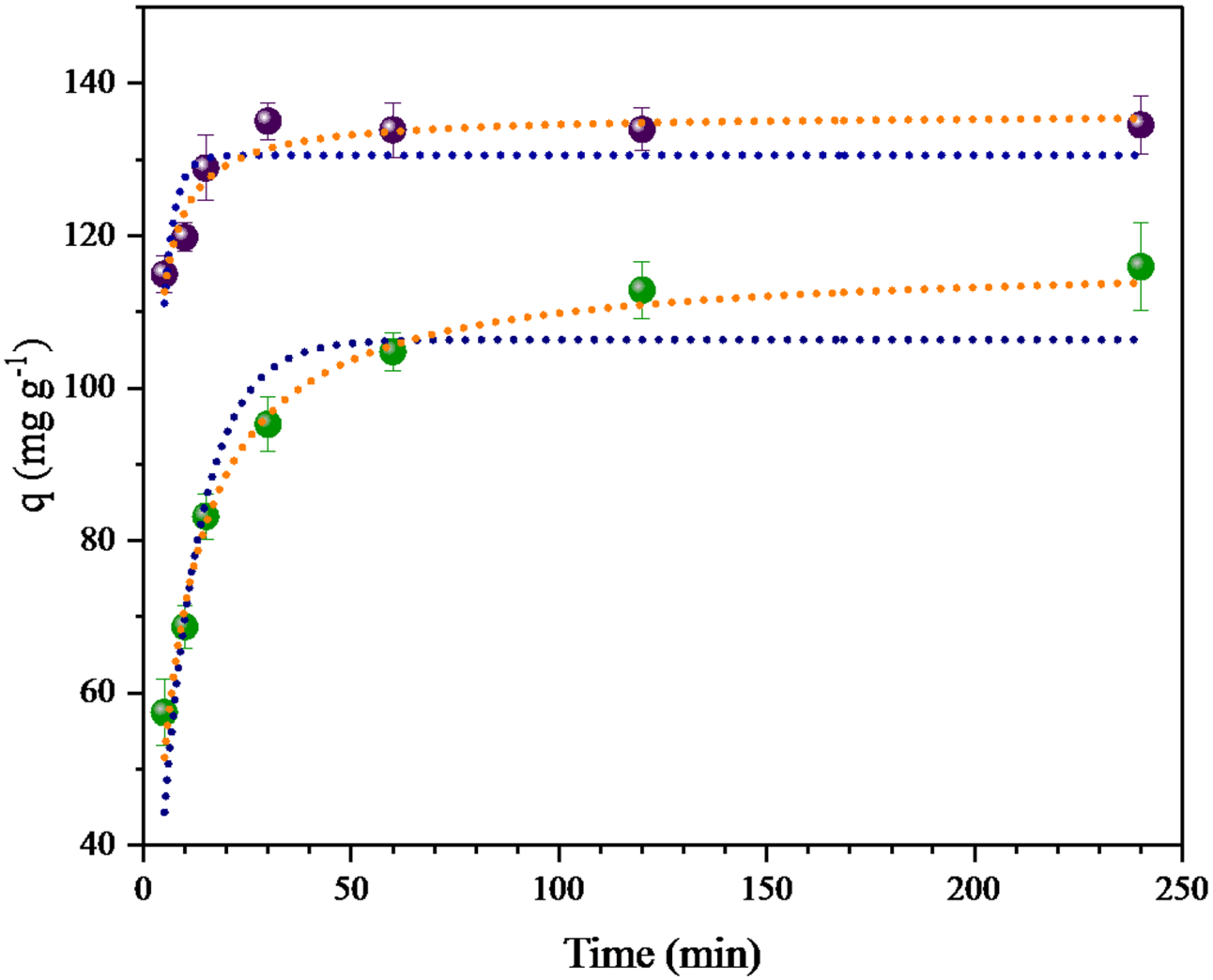

Fig. 6. Effect of contact time (Ci = 150 ppm, m = 30 mg, V = 30 mL, T = 25 °C, stirring speed = 110 rpm).

Samples		Pseudo-first order			Pseudo-second order		
	$q_{e,exp}$	k_1	$q_{e,cal}$	R^2	k_2	$q_{e,cal}$	R^2
HGC	115.96	0.1078	106,3674	0.91	0.0013	116.8081	0.99
HGC-LAP	134.56	0.3808	130,5862	0.58	0.0071	135.9991	0.97

Table 1. The parameters of the pseudo-first order and pseudo-second order kinetic model.

The adsorption process between the dye and the nanocomposites occurred through electrostatic attractions and hydrogen bonds, due to the presence of carboxylate groups in the hydrogel structure and an amine group present in the dye[45,46]. The schematization of the adsorption process can be seen in Fig. 7.

pH_{pcz} and pH influence

The point of zero charge (pH_{pcz}) indicates the pH where the surface charge is zero. At pHs below pHpcz the surface charge has a more cationic character, while at pHs above pH_{pcz} it has an anionic character. The study of pH_{pcz} becomes a fundamental parameter for the study of adsorption, as the surface charge of the adsorbent material can behave in different ways according to the pH of the medium[47,48].

The pH_{pcz} of the hydrogels were checked to evaluate the surface behavior as a function of pH. The balance point of the charges was determined at pH 11.25 and 11.46 for HGC and HGC-LAP, respectively, as shown in Fig. 8a. The clay mineral did not significantly influence the pH_{pcz}, due to the low concentration used of only 2%, in addition, as discussed by Gao et al., (2021), the increase in laponite concentration favored this small increase in negative charges in the system, indicating that laponite did not cause changes in charges in the

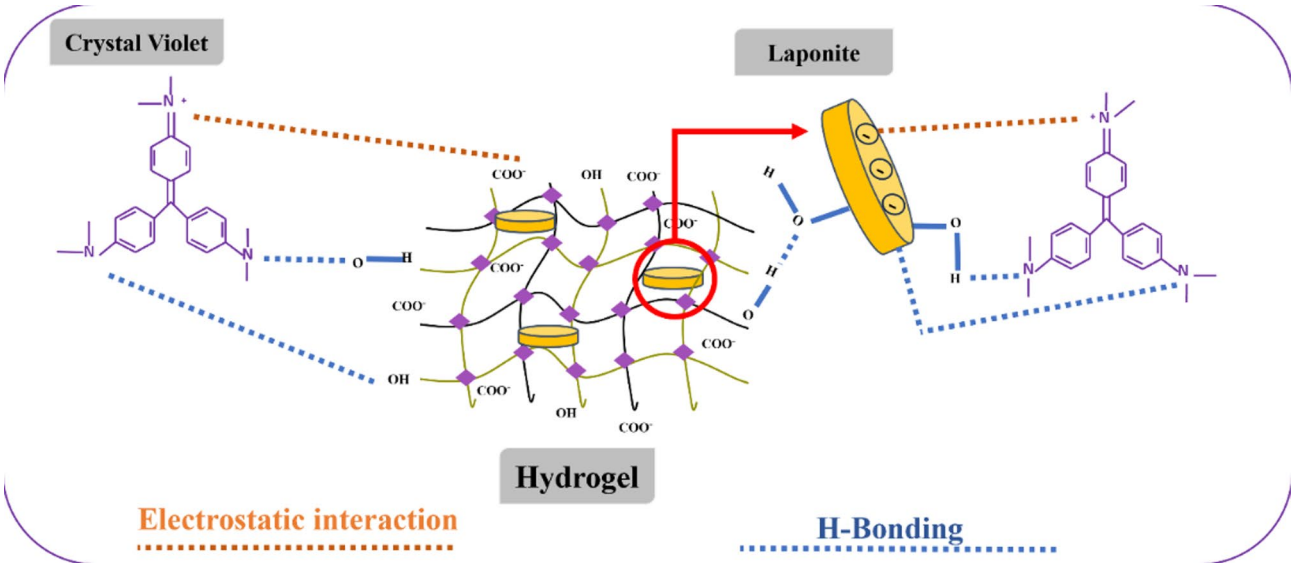

Fig. 7. Illustration of the interaction mechanism between the nanocomposite and the crystal violet dye.

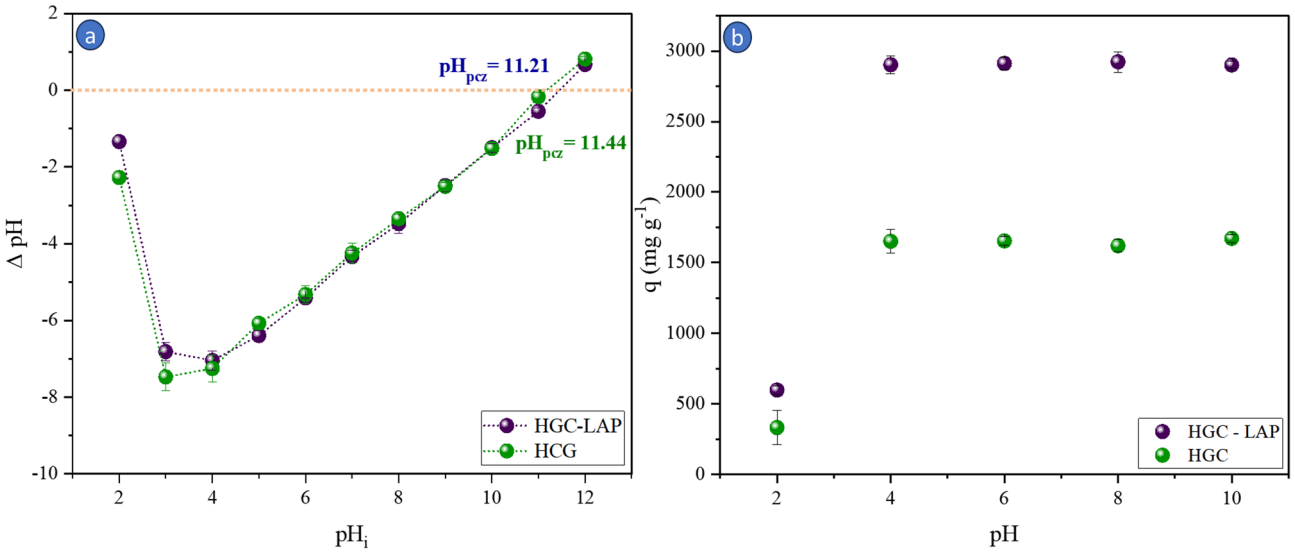

Fig. 8. (a) Zero charge point for HCG and (b) HCG-LAP Study of the effect of pH on HCG and HCG-LAP (Ci = 3000 ppm, m = 30 mg, V = 30 mL, T = 25 °C, stirring speed = 110 rpm).

system, generating a tendency greater interaction with cationic molecules upon contact with the nanocomposite, due to the adsorption capacity at pH < pH_{pcz}.

Due to the basic character of the surface charge of hydrogels, there is a tendency for greater affinity in the adsorption of cationic solutes from aqueous media[49–51].

The effect of pH on the adsorption of the cationic dye Violeta Cristal was analyzed for the HGC and HGC-LAP materials at pHs in the range 2 to 10, with a contact time of 2 h. pH is one of the most important parameters to be investigated, as it affects the surface charge of active sites and the distribution of the dye in aqueous solution[7]. Figure 8b displays the results obtained for the two materials, indicating that the addition of clay mineral does not change the adsorption capacity with pH variation, but increases the adsorption capacity with the addition of Laponite, since the laponite is loaded negatively and will be favored when interacting with systems containing negative charges[52]. At pH 2, hydrogels exhibit a lower adsorption rate due to protonation of -COO- groups, thus preventing interaction between the cationic groups of the dye. Furthermore, at pH 2, the hydrogel chain retracts, contributing to a reduction in adsorption capacity[52].

At pH below 4 most -COO- are protonated forming -COOH, as a result, the interaction between hydrogen bonds increases promoting a physical cross-linking, while the repulsion between -COO- is restricted, causing a shrinkage of the polymeric network and as a result, the adsorption capacity is reduced[11,12,52].

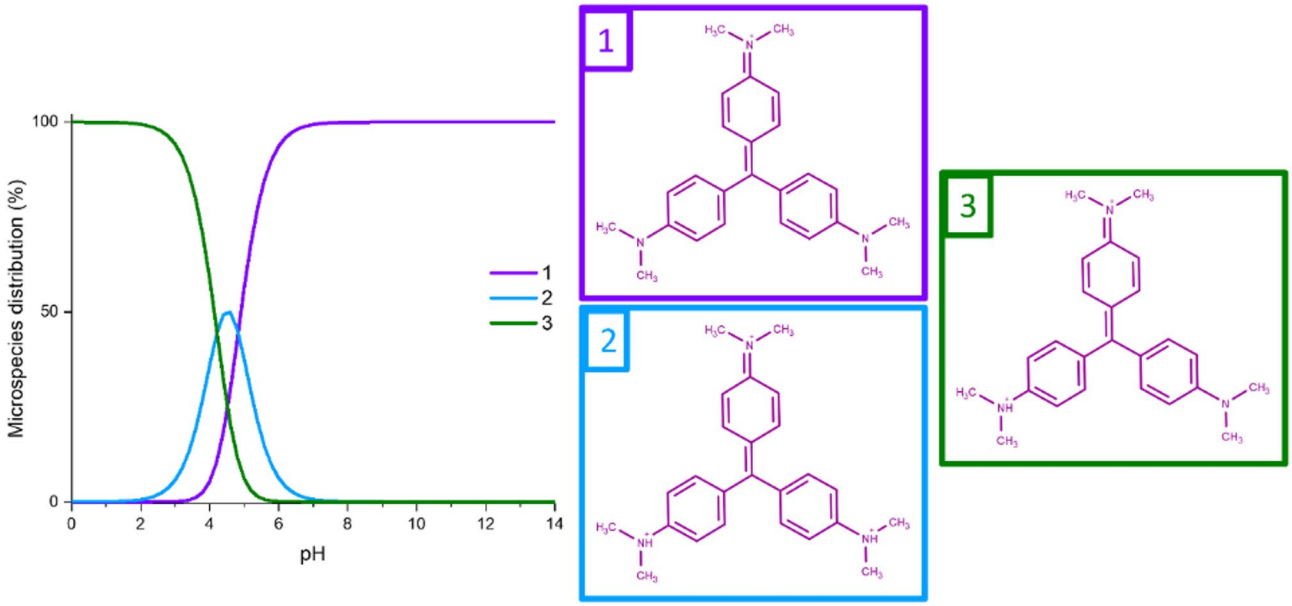

Fig. 9. Percentage of micro species of crystal violet dye with pH variation.

Isotherm model	Parameter	R^2	Parameter	R^2
	HGC		HGC-LAP	
Langmuir	q_m= 1760.62 K_L=0.0158	0.99	q_m= 3083.3807 K_L= 0.2707	0.99
Freundlich	K_F= 306.9376 *n* = 4.2384	0.78	K_F=451.0330 *n* = 3.4799	0.84
Redlich-Peterson	K_R= 20.5823 α_R = 0.0054 β = 0.9911	0.99	K_R=69.6815 α_R = 0.0123 β = 1.009	0.99
Sips	Q_{max}= 1760.5791 K_S= 0.0158 *n* = 2.4533	0.98	Q_{max}=3083.2120 K_S=0.2708 *n* = 1.5743	0.99
Temkin	A = 0.2900 B = 290.4799	0.91	A = 0.4716 B = 510.7857	0.95
Dubinin-Radushkevich	q_m= 1521.5552 β = 1623.1753	0.91	q_m=2786.4417 β = 634.4833	0.94

Table 2. Adsorption isotherm data for HGC and HGC-LAP.

The hydrogels presented a wide range for adsorption of cationic dyes, ranging from 2 to pH 11.44, as observed in pH_{pcz} where the lowest adsorption capacity was at pH 2 due to the protonation of the -COO- groups present in the polymeric structure and the negatively charged surface of laponite. Therefore, the presence of a greater number of H^+ ions leads to competition with the crystal violet dye for the adsorption process[25]. Despite lower adsorption at pH 2, it is important to highlight that low adsorption did not occur, as HGC showed adsorption of 332.90 mg g^{-1} while HGC-LAP showed 606.96 mg g^{-1}.

Even in a structure containing protonated groups, the interaction between the amine groups of the crystal violet dye and the protonated groups exists, but with greater restriction[7]. With the deprotonation of these groups, there is a greater repulsion between the anions of the polymeric network, in addition to increasing the difference in osmotic pressure between the adsorbent and adsorbate, promoting greater adsorption.

The crystal violet dye has 3 chemical species with varying pH. When crystal violet is at a pH below 1, the three nitrogen atoms in the structure acquire a positive charge, with two of these atoms in protonated form. At pHs close to 2, the dye undergoes deprotonation and the molecule has two positive charges. For pH above 4, chemical species 2 (with 1 protonated nitrogen) and 1 (without protonation) are dominant, favoring interaction with other cationic molecules. Furthermore, at pH 5 the dominance of species 1 occurs, being 100% at pHs above 7. The species distribution graph for the crystal violet dye can be seen in Fig. 9.

Adsorption isotherms

Isotherms describe the relationship between the dye adsorption capacity in the hydrogel matrix and the dye concentration under equilibrium conditions. The maximum adsorption capacity was observed at 1648.2 mg g^{-1} for HGC and 2887.5 mg g^{-1} for HGC-LAP, as shown in Table 2.

The relationship between the amount of dye adsorbed and the equilibrium concentration after the adsorption process can be expressed through mathematical relationships using adsorption isotherms. Among the adsorption models, the Langmuir and Freundlich models are widely used to understand the adsorption mechanism[7,10,41,42]. The Langmuir model is the most common in the literature, assuming that adsorption occurs through a monolayer process, meaning there is a finite number of adsorption sites on the adsorbent materials, with equivalent energies, without lateral interactions between adjacent molecules, and forming a single layer[47]. In contrast, the Freundlich isotherm assumes that adsorption occurs in multilayers and is one of the oldest known adsorption models. The Freundlich model is not limited to monolayers and considers a non-uniform distribution due to distinct affinities across a heterogeneous surface.

The equilibrium adsorption graph is characterized by a rapid initial adsorption, where the highest energy binding sites are the first to be occupied. After this initial phase, the energy involved in adsorption decreases exponentially as the process progresses and the remaining adsorption sites are filled[1].

As shown in Table 2; Fig. 10, the experimental data were better fitted to the Langmuir model for both hydrogels, with an R^2 of 0.99 for both HGC and HGC-LAP. On the other hand, the Freundlich model's linear coefficient was 0.78 for HGC and 0.84 for HGC-LAP, indicating that adsorption predominantly follows the monolayer model. Additionally, the Redlich-Peterson model was also used, presenting a linear coefficient of 0.99 and a β value close to 1 for both materials, as indicated in Table 2. These results suggest that the adsorption behavior is consistent with the Langmuir model, showing a predominance of monolayer adsorption with minimal heterogeneity[35]. The data also fit well with the Sips model, which presented maximum adsorption values and constants identical to those of the Langmuir model for both materials, reinforcing the monolayer mechanism. The n value greater than 1 in the Sips isotherm indicates cooperative behavior, reflecting a predominance of monolayer adsorption with an additional contribution of heterogeneity[36].

The data did not fit well with the Temkin and Dubinin-Radushkevich models, due to the low correlation coefficients for both materials, reinforcing that the adsorption mechanism occurs through chemical interactions.

Selective adsorption

A mixture of dyes with opposite charges was prepared, namely, crystal violet with a positive charge and methyl orange with a negative charge, both at a concentration of 50 ppm. Figure 11a shows the UV-Vis spectrum of the crystal violet (λ = 583 nm) and methyl orange (λ = 464 nm) dyes, as well as the spectrum of the mixture of the two dyes at the same concentration of 50 ppm. Figure 11b shows the spectrum of the dye mixture solution after the adsorption process with HGC and HGC-LAP, both after a period of 120 min.

As seen in Fig. 11b, it is observed that, after adsorption, the band corresponding to methyl orange showed a small reduction in absorption, while there was a considerable reduction in the band of crystal violet. This indicates that HGC and HGC-LAP exhibit selective removal for the cationic dye used as a model in this study, demonstrating that the material has a high affinity for removing positively charged solutes.

The hydrogel containing laponite showed a greater selective adsorption capacity compared to the hydrogel without laponite, as seen in Fig. 11b. While HGC-LAP adsorbed 92.3% of the crystal violet dye, HGC adsorbed 71.8% under the same adsorption conditions. The hydrogels did not show good adsorption for the anionic methyl orange dye, with removal percentages of 8.92% and 9.56%, respectively, consistent with the results obtained by pH_{pcz}, where the nanocomposites have a preferential adsorption for cationic molecules.

It is of great importance that an adsorbent material has reusability, as this ensures a sustainable approach for its large-scale use[53]. During the reuse study, the crystal violet dye adsorbed on the hydrogels needs to be

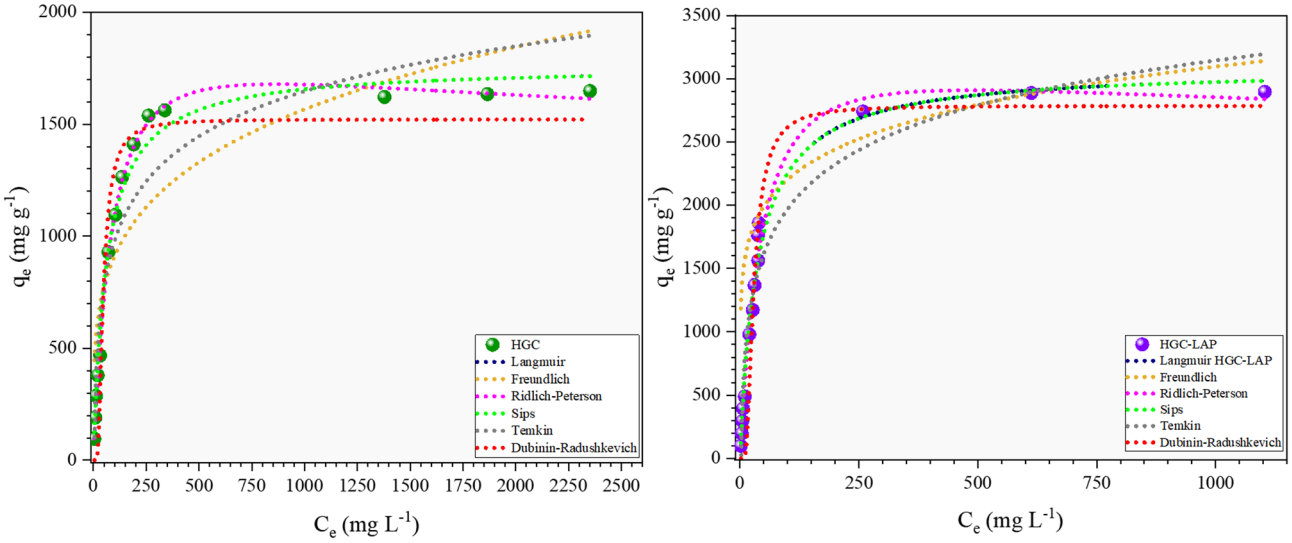

Fig. 10. Experimental data and fitting of different isotherm models for HCG and HCG-LAP (Ci = 3000 ppm, m = 30 mg, V = 30 mL, T = 25 °C, stirring speed = 110 rpm).

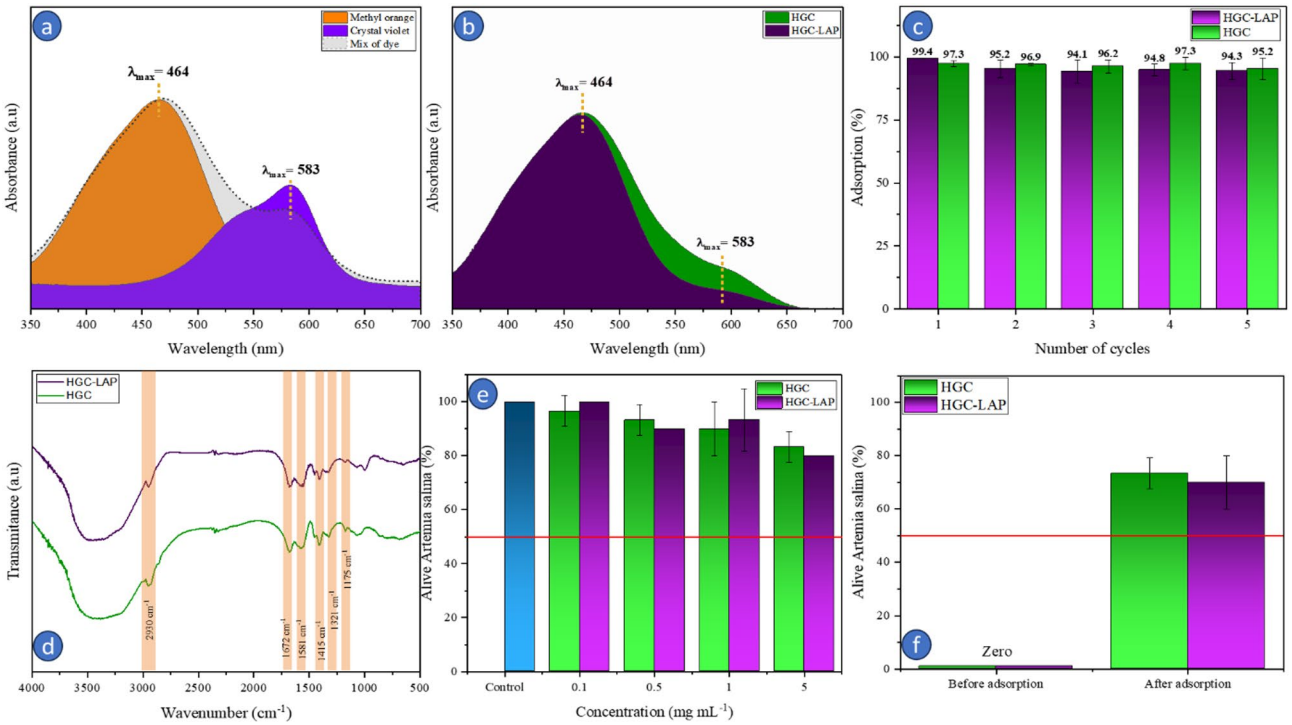

Fig. 11. (a) Absorption bands in the UV-Vis region for the methyl orange, crystal violet and mixture of methyl orange and crystal violet dyes (b) Spectrum after adsorption of the dye mixture with HGC and HGC-LAP, (c) Adsorption percentage after 5 cycles of adsorption and desorption of crystal violet dye for HGC and HGC-LAP, (d) Fourier transform infrared (FTIR) spectra of HGC-LAP, HGC and LAP after adsorption of crystal violet dye, (e) Toxicity bioassay against Artemia Salina hydrogels before and (f) after adsorption of crystal violet dye.

desorbed so that the active sites of the hydrogels are available for other adsorption cycles. The reuse data is depicted in Fig. 11c.

The reuse process was carried out using ethanol[1]. In the presence of ethanol, the hydrophilic functional groups of ethanol (OH) firmly adsorb onto the hydrogel surface, unlike the method proposed by[53], where the interaction occurs directly with the dye. As a result of the interaction of ethanol with the hydrogel surface, desorption of these molecules occurs, making the material reusable.

As shown in Fig. 11c, during reuse cycles, the adsorption capacity of hydrogels decreases. This occurs due to the blocking of some active sites by dye molecules adsorbed with strong chemical interactions[1]. Given the high removal capacity even after 5 reuse cycles, it is suggested that the hydrogel shows good stability in consecutive adsorption and desorption processes, with small variations within the margin of error and without differences in measurements due to the presence of clay.

FTIR analysis was used after the adsorption process to investigate the presence of chemical interactions between the dye and hydrogels.

The crystal violet dye presents characteristic bands at 1592 cm^{-1} for stretching of the C = C aromatic ring, 1175 cm^{-1} referring to the C-N stretching, 2915 cm^{-1} for stretching of the C-H group and 1360 cm^{-1} referring to the C-N stretching of the tertiary amine group stretching[1].

Figure 11d shows the FTIR spectrum after the adsorption process. It is possible to observe the presence of characteristic bands of the crystal violet dye at 1581 and 1175 cm^{-1}. From Fig. 11d it is possible to observe the shift of the band from 1360 cm^{-1} to 1321 cm-1 and 1443 cm^{-1} to 1415 cm^{-1} indicating the interaction between the hydrogel and the dye[1]. Furthermore, the bands at 2915 cm^{-1} are not observed due to the proximity of the asymmetric and symmetric C-H stretching present in the biopolymer located at 2930 cm^{-1}.

The bioassay against *Artemia salina* was carried out over a period of 48 h with HGC and HGC-LAP in addition to analyzing the solution after the adsorption process of the two materials, as shown in Fig. 11e. According to the safety profile presented by[28], the hydrogels did not show toxicity against Artemia salina, since the mortality rate shown by the bioassay was less than 50% in both hydrogels before and after the adsorption process.

As seen in Fig. 11e, after 48 h the mortality rate still remained below 50% even at a concentration of 5 mg mL^{-1} for the hydrogels before the adsorption process. Similar results were obtained[12]. In the post adsorption process, Fig. 11f, it was observed that the dye concentration in the water was lower than 5 ppm (C_e = 5ppm), resulting in a mortality rate lower than 70% and without the presence of toxicity, indicating that the solution After adsorption of the dye, it showed no toxicity.

Adsorbent	Dye	q_{max} (mg g^{-1})	Reference
Carrageenan-based hydrogel containing laponite	Crystal violet	79.8	[54]
Xanthan Gum Hydrogels		502.0	[55]
TiO_2 hydrogel based on sodium alginate grafted with acrylic acid		1156.6	[56]
Acrylic acid/vermiculite hydrogels		1989.5	[7]
Nanocomposite hydrogels of carrageenan and sodium alginate and montmorillonite		88.8	[57]
Cashew gum tree nanocomposite hydrogels		1648.2	This work
Cashew gum tree/laponite nanocomposite hydrogels		2887.5	This work

Table 3. Comparative table of the adsorption capacity of hydrogels on cationic dyes.

Therefore, the hydrogels produced with and without the use of laponite appear to be good adsorbents of the crystal violet dye, presenting the capacity to adsorb enough molecules to make the environment an environment with reduced toxicity, considering the toxicity safety profile against *A. salina* presented by[28].

Comparison of adsorption data with other hydrogels

To verify the advantage of the hydrogels produced in these studies using hybrid chain with the addition of laponite for adsorption of cationic dyes, the maximum adsorption capacity was compared with hydrogels reported in the literature. The adsorption comparison can be seen in Table 3.

Conclusion

The synthesis of the hydrogels with and without laponite was successfully carried out and characterized using XRD, FTIR, SEM, and TG techniques. FTIR analysis revealed characteristic bands related to cashew gum and polyacrylamide, such as the asymmetric and symmetric stretching of C = O and N-H present in polyacrylamide at 1669 cm^{-1}, and C-H corresponding to the biopolymer at 2930 cm^{-1}. XRD analysis identified an intermediate profile between the crystalline profile of cashew gum and acrylamide, related to the macromolecular chain grafting reaction. Additionally, characteristic peaks of Laponite were identified in the HGC-LAP samples, indicating that a cross-linking reaction occurred in this hydrogel with preservation of both amorphous and crystalline phases. Thermogravimetric analysis confirmed the presence of clay mineral in the nanocomposite, evidenced by new thermal events and reduced mass loss in HGC-LAP, proportional to the amount of laponite added. SEM analysis revealed higher density in the laponite-containing material, as well as good homogeneity observed in the EDS mapping. The inorganic phase also influenced the swelling capacity of the hydrogel, as there was an increase in cross-linking, leading to greater resistance to water absorption. HGC and HGC-LAP had a pH_{pcz} of 11.25 and 11.46, respectively, with no significant difference in surface charge, but there was a significant increase in the adsorption capacity of cationic dyes due to the presence of laponite in HGC-LAP. The hydrogels showed stability in dye adsorption in the pH range above 4, with a maximum adsorption of 1,648.2 mg g^{-1} for HGC and 2,887.5 mg g^{-1} for HGC-LAP at pH 6. The experimental data were better fitted to the pseudo-second-order model for both hydrogels, and the isothermal model was Langmuir. The hydrogels demonstrated selectivity in dye adsorption, with a preference for cationic dyes due to the characteristics of the groups available for interaction.

Data availability

The methodology section provides details about the materials used, including the nanocomposite hydrogels and dyes. This section contains all the necessary information for replicating the materials and conducting the experiments according to the described methods. Additionally, the datasets used and/or analyzed during the study are available upon request from the corresponding author.

Received: 16 October 2024; Accepted: 16 May 2025
Published online: 01 July 2025

References

1. Sharma, S. et al. Adsorption of cationic dyes onto Carrageenan and Itaconic acid-based superabsorbent hydrogel: synthesis, characterization and isotherm analysis. *J Hazard. Mater* **421**, (2022).
2. Shen, B. et al. Preparation of hydrogels based on pectin with different esterification degrees and evaluation of their structure and adsorption properties. *Int. J. Biol. Macromol.* **202**, 397–406 (2022).
3. Xu, S., Jin, Y., Li, R., Shan, M. & Zhang, Y. Amidoxime modified polymers of intrinsic microporosity/alginate composite hydrogel beads for efficient adsorption of cationic dyes from aqueous solution. *J. Colloid Interface Sci.* **607**, 890–899 (2022).
4. Mohammadzadeh Pakdel, P. & Peighambardoust, S. J. A review on acrylic based hydrogels and their applications in wastewater treatment. *Journal of Environmental Management* vol. 217 123–143 Preprint at (2018). https://doi.org/10.1016/j.jenvman.2018.03.076
5. Mohammadzadeh Pakdel, P. & Peighambardoust, S. J. Review on recent progress in chitosan-based hydrogels for wastewater treatment application. *Carbohydrate Polymers* vol. 201 264–279 Preprint at (2018). https://doi.org/10.1016/j.carbpol.2018.08.070
6. Tan, K. B. et al. Adsorption of dyes by nanomaterials: Recent developments and adsorption mechanisms. *Separation and Purification Technology* vol. 150 229–242 Preprint at (2015). https://doi.org/10.1016/j.seppur.2015.07.009
7. Lu, Q. et al. Synthesis and adsorption properties for cationic dyes of acrylic acid/vermiculite hydrogel initiated by Glow-Discharge-Electrolysis plasma. *Adv. Polym. Technol.* **37**, 996–1007 (2018).

8. Peighambardoust, S. J., Azari, M. M., Pakdel, P. M., Mohammadi, R. & Foroutan, R. Carboxymethyl cellulose grafted poly(acrylamide)/magnetic Biochar as a novel nanocomposite hydrogel for efficient elimination of methylene blue. *Biomass Convers. Biorefin*. https://doi.org/10.1007/s13399-024-06180-2 (2024).
9. Peighambardoust, S. J. et al. Effectiveness of polyacrylamide-g-gelatin/ACL/Mg-Fe LDH composite hydrogel as an eliminator of crystal Violet dye. *Environ Res* **258**, (2024).
10. Mittal, H., Kumar, V., Ray, S. S. & Saruchi & Adsorption of Methyl Violet from aqueous solution using gum xanthan/Fe3O4 based nanocomposite hydrogel. *Int. J. Biol. Macromol.* **89**, 1–11 (2016).
11. Şolpan, D. & Kölge, Z. Adsorption of Methyl Violet in aqueous solutions by poly(N- vinylpyrrolidone-co-methacrylic acid) hydrogels. *Radiat. Phys. Chem.* **75**, 120–128 (2006).
12. Rodrigues, H. et al. Superabsorbent hydrogels based to Polyacrylamide/Cashew tree gum for the controlled release of water and plant nutrients. *Molecules* **26**, 2680 (2021).
13. Chen, M., Shen, Y., Xu, L., Xiang, G. & Ni, Z. Highly efficient and rapid adsorption of methylene blue dye onto vinyl hybrid silica nano-cross-linked nanocomposite hydrogel. *Colloids Surf. Physicochem Eng. Asp* **613**, (2021).
14. Etemadi Baloch, F., Afzali, D. & Fathirad, F. Design of acrylic acid/nanoclay grafted polysaccharide hydrogels as superabsorbent for controlled release of Chlorpyrifos. *Appl. Clay Sci.* **211**, 106194 (2021).
15. Andrade, K. C. S. et al. Goma de Cajueiro (Anacardium occidentale): Avaliação Das modificações Químicas e físicas Por extrusão termoplástica. *Polimeros* **23**, 667–671 (2013).
16. Oliveira, E. F., Paula, H. C. B. & Paula, R. C. M. De. Alginate/cashew gum nanoparticles for essential oil encapsulation. *Colloids Surf. B Biointerfaces*. **113**, 146–151 (2014).
17. Koyyada, A. & Orsu, P. Natural gum polysaccharides as efficient tissue engineering and drug delivery biopolymers. *J. Drug Deliv Sci. Technol.* **63**, 102431 (2021).
18. Ribeiro, A. J. et al. Gums' based delivery systems: Review on cashew gum and its derivatives. *Carbohydrate Polymers* vol. 147 188–200 Preprint at (2016). https://doi.org/10.1016/j.carbpol.2016.02.042
19. Mohammadzadeh Pakdel, P., Sayyar, Z. & Peighambardoust, S. J. Remediation of basic dyes using cloisite 30B embedded carboxymethyl cellulose grafted acrylic acid and Itaconic acid nanocomposite hydrogela. *Polym. Bull.* https://doi.org/10.1007/s00289-024-05361-3 (2024).
20. Foroughi, M., Peighambardoust, S. J., Ramavandi, B., Foroutan, R. & Peighambardoust, N. S. Simultaneous degradation of Methyl orange and Indigo Carmine dyes from an aqueous solution using nanostructured WO3 and CuO supported on zeolite 4A. *Sep Purif. Technol* **344**, (2024).
21. Afewerki, S. et al. Bioprinting a synthetic smectic clay for orthopedic applications. *Adv. Healthc. Mater.* **8**, 1–14 (2019).
22. Huang, H., Liu, Z., Yun, J., Yang, H. & Xu, Z. liang. Preparation of laponite hydrogel in different shapes for selective dye adsorption and filtration separation. *Appl Clay Sci* **201**, (2021).
23. Peighambardoust, S. J., Karimzadeh Halimi, F., Mohammadzadeh Pakdel, P. & Safarzadeh, H. Decontamination of methylene blue from aqueous media using alginate-bonded polyacrylamide/carbon black nanocomposite hydrogel. *Polym Adv. Technol* **35**, (2024).
24. Alizadeh, M., Peighambardoust, S. J. & Foroutan, R. Efficacious adsorption of divalent nickel ions over sodium alginate-g-poly(acrylamide)/hydrolyzed Luffa cylindrica-CoFe2O4 Bionanocomposite hydrogel. *Int J. Biol. Macromol* **254**, (2024).
25. Gao, B. et al. Super-adsorbent poly(acrylic acid)/laponite hydrogel with ultrahigh mechanical property for adsorption of methylene blue. *J Environ. Chem. Eng* **9**, (2021).
26. Rodrigues, J., Paula, R., Tecnologia, S. C. P. & ciência e & U. Methods of isolation of natural gums: comparison through cashew gum (Anacardium occidentale L.). Original title: Métodos de isolamento de gomas. *Polímeros: ciência e tecnologia* 1, 31–36 (1993). (1993).
27. Tanan, W., Panichpakdee, J. & Saengsuwan, S. Novel biodegradable hydrogel based on natural polymers: synthesis, characterization, swelling/reswelling and biodegradability. *Eur. Polym. J.* **112**, 678–687 (2019).
28. Meyer, B. N. et al. Brine shrimp: A convenient general bioassay for active plant constituents. *Planta Med.* **45**, 31–34 (1982).
29. LAGERGREN, S. Zur theorie der sogenannten adsorption gelöster Stoffe. *Z. Für Chemie Und Ind. Der Kolloide*. **2**, 15–15 (1907).
30. Ho, Y. S. & Mckay, G. Pseudo-Second order model for sorption processes. *Process Biochem.* **34** (1999).
31. Langmuir, I. The constitution and fundamental properties of solids and liquids. *J. Frankl. Inst.* **183**, 102–105 (1917).
32. Freundlich, H. Über die adsorption in lösungen. *Z. FÃ¼r Phys. Chem.* **57U**, 385–470 (1907).
33. Jossens, L., Prausnitz, J. M., Fritz, W., Schlünder, E. U. & Myers, A. L. Thermodynamics of multi-solute adsorption from dilute aqueous solutions. *Chem. Eng. Sci.* **33**, 1097–1106 (1978).
34. Sips, R. On the structure of a catalyst surface. *J. Chem. Phys.* **16**, 490–495 (1948).
35. Senthil Kumar, P. et al. Adsorption of dye from aqueous solution by cashew nut shell: studies on equilibrium isotherm, kinetics and thermodynamics of interactions. *Desalination* **261**, 52–60 (2010).
36. Volesky, B. Biosorption process simulation tools. in *Hydrometallurgy* vol. 71 179–190 (2003).
37. Daniel, L. M., Frost, R. L. & Zhu, H. Y. Edge-modification of laponite with dimethyl-octylmethoxysilane. *J. Colloid Interface Sci.* **321**, 302–309 (2008).
38. Ferreira, S. R. et al. Sustainable natural gums for industrial application: physiochemical and texturometric evaluation. *J Drug Deliv Sci. Technol* **54**, (2019).
39. Giannakas, A. A., Giannakas, A. A. & Ladavos, A. Preparation and characterization of polystyrene/organolaponite nanocomposites. *Polym. Plast. Technol. Eng.* **51**, 1411–1415 (2012).
40. Zhang, X., Han, M., Fuseni, A. & Alsofi, A. M. An approach to evaluate polyacrylamide-type polymers' long-term stability under high temperature and high salinity environment. *J. Pet. Sci. Eng.* **180**, 518–525 (2019).
41. Haraguchi, K., Takehisa, T. & Fan, S. Effects of clay content on the properties of nanocomposite hydrogels composed of poly(N-isopropylacrylamide) and clay. *Macromolecules* **35**, 10162–10171 (2002).
42. Haraguchi, K. & Takehisa, T. Nanocomposite hydrogels: A unique organic-inorganic network structure with extraordinary mechanical, optical, and swelling/De-swelling properties. *Adv. Mater.* **14**, 1120–1124 (2002).
43. Wang, J. et al. Adsorption properties of β-cyclodextrin modified hydrogel for methylene blue. *Carbohydr Res* **501**, (2021).
44. Peighambardoust, S. J., Ghergherehchi, E., Mohammadzadeh Pakdel, P. & Aghdasinia, H. Facile removal of methylene blue using carboxymethyl cellulose grafted polyacrylamide/carbon black nanocomposite hydrogel. *J. Polym. Environ.* **31**, 939–953 (2023).
45. Safarzadeh, H., Peighambardoust, S. J. & Peighambardoust, S. H. Application of a novel sodium alginate-graft-poly(methacrylic acid-co-acrylamide)/montmorillonite nanocomposite hydrogel for removal of malachite green from wastewater. *Journal Polym. Research* **30**, (2023).
46. Safarzadeh, H., Peighambardoust, S. J., Mousavi, S. H., Mohammadi, R. & Peighambardoust, S. H. Adsorption of Methyl Violet dye from wastewater using poly(methacrylic acid-co-acrylamide)/bentonite nanocomposite hydrogels. *Journal Polym. Research* **29**, (2022).
47. Appel, C., Ma, L. Q., Rhue, R. D. & Kennelley, E. Point of zero charge determination in soils and minerals via traditional methods and detection of electroacoustic mobility. *Geoderma* **113**, 77–93 (2003).
48. Zhao, Y., Liu, F. & Qin, X. Adsorption of diclofenac onto goethite: adsorption kinetics and effects of pH. *Chemosphere* **180**, 373–378 (2017).
49. Foroutan, R., Peighambardoust, S. J., Mohammadi, R., Ramavandi, B. & Boffito, D. C. One-pot transesterification of non-edible Moringa oleifera oil over a MgO/K2CO3/HAp catalyst derived from poultry skeletal waste. *Environ Technol Innovation* **21**. https://doi.org/10.1016/j.eti.2020.101250 (2021).

50. Rowshanzamir, S., Peighambardoust, S. J., Parnian, M. J., Amirkhanlou, G. R. & Rahnavard, A. Effect of Pt-Cs2.5H0.5PW12O40 catalyst addition on durability of self-humidifying nanocomposite membranes based on sulfonated poly (ether ether ketone) for proton exchange membrane fuel cell applications. *Int J Hydrogen Energy* **40**, 549–560. https://doi.org/10.1016/j.ijhydene.2014.10.134 (2015).
51. Safarzadeh, H. et al. Adsorption ability evaluation of the poly(methacrylic acid-co-acrylamide)/cloisite 30B nanocomposite hydrogel as a new adsorbent for cationic dye removal. *Environ Res* **212**. https://doi.org/10.1016/j.envres.2022.113349 (2022).
52. Edvan, R. et al. Copolymerized natural fibre from the mesocarp of Orbignya phalerata (babassu fruit) as an irrigating-fertilizer for growing cactus Pears. *Polym. (Basel).* **12**, 1699 (2020).
53. Kumari, S., Chowdhury, A., Khan, A. A. & Hussain, S. Controlled surface functionalization of Ni-S nanostructures for pH-responsive selective and superior pollutants adsorption. *J. Hazard. Mater.* **415**, 125750 (2021).
54. Mahdavinia, G. R., Massoudi, A., Baghban, A. & Massoumi, B. Novel carrageenan-based hydrogel nanocomposites containing laponite RD and their application to remove cationic dye. *Iran. Polym. J. (English Edition).* **21**, 609–619 (2012).
55. Njuguna, D. G. & Schönherr, H. Xanthan gum hydrogels as High-Capacity adsorbents for dye removal. *ACS Appl. Polym. Mater.* **3**, 3142–3152 (2021).
56. Thakur, S. & Arotiba, O. Synthesis, characterization and adsorption studies of an acrylic acid-grafted sodium alginate-based TiO2 hydrogel nanocomposite. *Adsorpt. Sci. Technol.* **36**, 458–477 (2018).
57. Mahdavinia, G. R. & Asgari, A. Synthesis of kappa-carrageenan-g-poly(acrylamide)/sepiolite nanocomposite hydrogels and adsorption of cationic dye. *Polym. Bull.* **70**, 2451–2470 (2013).

Acknowledgements

The authors would like to thank the Coordination for the Improvement of Higher Education Personnel – CAPES and Piauí State Research Support Foundation – FAPEPI (Nº 23038.006531/2021-17). This work was partially supported by Brazilian agencies MCTIC/CNPq (Grant #406973/2022-9 - INCT/Polysaccharides (National Technology-Science Institute for Polysaccharides; 308434/2023-4; 406050/2022-8).

Author contributions

Albert Santos Silva: Conceptualization, Methodology, Validation, Investigation, Formal analysis, Writing - Original Draft, Ariane Maria Silva Santos: Investigation, Validation, Visualization. Josy Anteveli Osajima: Writing - Review & Editing, Visualization, Funding acquisition. Edvani Curti Muniz: Writing - Review & Editing, Visualization, Funding acquisition. Monica Felts de La Roca Soares: Writing - Review & Editing, Visualization. Rafael Felippe Ratke: Writing - Review & Editing. Natielly Pereira da Silva: Writing - Review & Editing. Edson C. Silva-Filho: Conceptualization, Writing - Review & Editing, Visualization, Supervision, Project administration, Funding acquisition.

Declarations

Competing interests

The authors declare no competing interests.

Additional information

Correspondence and requests for materials should be addressed to E.C.S.-F.

Reprints and permissions information is available at www.nature.com/reprints.

Publisher's note Springer Nature remains neutral with regard to jurisdictional claims in published maps and institutional affiliations.